Polarization observables in exclusive kaon photoproduction on the deuteron

K. Miyagawa

Department of Applied Physics, Okayama University of Science

1-1 Ridai-cho, Okayama 700, Japan

T. Mart

Departemen Fisika, FMIPA, Universitas Indonesia, Depok 16424, Indonesia

C. Bennhold

Center for Nuclear Studies, Department of Physics,

The George Washington University, Washington, D.C. 20052, USA

W. Glöckle

Institut für Theoretische Physik II,

Ruhr-Universität Bochum, D-44780 Bochum, Germany

Abstract

Single and double polarization observables for kaon photoproduction on the deuteron are studied theoretically with modern hyperon-nucleon forces. The kinematical region of the kaon scattered forward with large momentum is thoroughly investigated where either the quasifree scattering leading to the kaon and hyperon or the final-state interaction between hyperon and nucleon are expected. The quasifree scatterings show characteristic peaks in the inclusive cross sections. The final-state interaction effects are significant, especially around the ΛN and ΣN thresholds. The double polarization C_z is found to be sensitive to the final-state interaction effects. Precise data would help to clarify the property of the ΛN-ΣN interaction and also help to extract the information on the elementary amplitude from the quasifree scattering region.

PACS numbers: 25.20.Lj, 13.75.Ev, 13.60.Le, 21.45.+v

I. INTRODUCTION

The hyperon-nucleon (YN) interaction has played a key role in hypernuclear physics. It is known as the basic force which binds Λ and Σ hyperons in hypernuclei. Even in a conventional nuclear system, understanding of the YN interaction is indisputably important if one introduces the strangeness degrees of freedom in the nucleon-nucleon (NN) interaction, in order to extend the baryon-baryon interaction to a more unified picture demanded by SU(3) symmetry.

While performing YN scattering experiments is a daunting task, hyperon photoproduction on the deuteron appears to be a promising process for investigating the available YN interaction models. This is made possible by choosing some photoproduction kinematics where the outgoing baryons have small relative momenta and, therefore, the YN interaction is effectively strong. Several previous studies have been done in inclusive and exclusive kaon photoproduction on the deuteron [1] based on simple YN forces. Nevertheless, all calculations indicated that significant YN final state interaction effects are present near the production thresholds.

Another motivation of performing experiments on the deuteron is due to the lack of the neutron target. Experiments for kaon photoproduction on the proton have just been finished in ELSA, JLab, and SPRING8, resulting in a large number of unprecedented precise data that certainly need more sophisticated analyses. However, previous studies [2, 3] had indicated that neutron channels can provide a more stringent constraint to elementary models that can successfully explain the process on the proton. Thus, kaon photoproduction on the deuteron can serve as a means for testing the available elementary models. To this end, a simple calculation has proven that in most kinematic situations the elementary cross section on the neutron can be reliably extracted from the deuteron cross section [4]. A related experiment has recently been done at LNS-Tohoku by measuring the K^0YN final states cross section and the collected data are being analyzed [5].

In the previous paper [6], we have investigated the inclusive K^+ and exclusive K^+Y photoproduction on the deuteron by using modern hyperon-nucleon forces and a certain kaon photoproduction operator. Sizable effects of the hyperon-nucleon final state interaction were found near the ΛN and ΣN thresholds in the inclusive reaction. Angular distributions for the exclusive process showed clear YN final state interaction effects in certain kinematic

regions. We pointed out that precise data especially for the inclusive process around the ΣN threshold would help to clarify the strength and property of the ΛN-ΣN interaction.

We notice that a fairly elaborate calculation focusing on rescattering contributions to the kaon photoproduction on the deuteron has recently appeared [7]. In order to emphasize the influence of rescattering terms in the differential cross sections, the calculation, however, has been performed in a certain kinematics where final state interactions among the hyperons and the nucleon have negligible effects. A more detailed calculation, which includes the YN and KN rescattering terms, as well as a two-body photoproduction contribution in terms of a pion mediated process $\gamma d \to \pi NN \to KYN$, has also been performed [8]. It is found that the latter gives the dominant contribution beyond the impulse approximation for backward kaon angles. In the forward directions ($\theta_K \lesssim 30^\circ$) the effects turn out to be small.

In this paper we theoretically examine in detail a number of polarization observables that are immediately accessible experimentally due to the high intensity continuous wave electron beams available nowadays at JLab, ELSA, GRAAL, and SPRING8, and due to the hyperon recoil polarization, which can be directly obtained from the hyperon decay. This work is also greatly motivated by the Hall A and Hall B data recently taken which are currently being analyzed [9, 10].

For the convenience of the reader we briefly describe the latest update of the elementary photoproduction operator in Sec. II. Section III describes the evaluation of the nuclear matrix element and the definition of various polarization observables. Our numerical results for the various YN forces are extensively given in Sec. IV and we give the conclusion in Sec. V.

II. THE ELEMENTARY PRODUCTION OPERATOR

Models for kaon photoproduction on the nucleon have been proliferating rapidly in recent years, due mostly to the continuously improving data base from experimental facilities like ELSA, GRAAL, and Jlab. Most of these descriptions employ an effective Lagrangian approach at tree level [3, 11, 12, 13] where the results from coupled-channel calculations [14] are taken into account. While the details of the model ingredients vary in the different studies, all models provide a good parameterization of the elementary kaon photoproduction data and are thus adequate for use in the nuclear environment.

Recently, we note that two new versions of data have just been published by the SAPHIR and the CLAS collaborations [15, 16]. Unfortunately, as reported in Ref. [16], the CLAS data show substantial and systematic discrepancies with the SAPHIR ones. Thus, as a consequence, an attempt to fit the model to both data simultaneously would be meaningless. While waiting for a new method to reconcile this problem, and for the sake of comparison, we will in this study use the same operator [17] we have used in our previous paper [6]. The operator consists of gauge-invariant background and resonances terms. The background terms include the standard s-, u-, and t-channel contributions along with a contact term required to restore gauge invariance after hadronic form factors have been introduced. The resonance part consists of three nucleon resonances that have been found in the coupled-channels approach to decay into the $K\Lambda$ channel, the $S_{11}(1650)$, $P_{11}(1710)$, and $P_{13}(1720)$. For the $K\Sigma$ production operator further contributions from the $S_{31}(1900)$ and $P_{31}(1910)$ Δ- resonances were added. In addition, we added the $D_{13}(1900)$ state [11] found to be important in the description of SAPHIR data [15, 18].

In order to implement the operator in a nuclear matrix element, we rewrite the amplitude in an arbitrary frame

$$
\begin{aligned}
t_{\gamma K} \;=\; & \left(\frac{E_N + m_N}{2m_N}\right)^{\frac{1}{2}} \left(\frac{E_Y + m_Y}{2m_Y}\right)^{\frac{1}{2}} \sqrt{\frac{m_Y}{E_Y}} \sqrt{\frac{m_N}{E_N}} \times \\
& \Big[\mathcal{F}_1\, \boldsymbol{\sigma}\cdot\boldsymbol{\epsilon} + \mathcal{F}_4\, \boldsymbol{\sigma}\cdot\boldsymbol{p}_\gamma\, \boldsymbol{p}_N\cdot\boldsymbol{\epsilon} + \mathcal{F}_5\, \boldsymbol{\sigma}\cdot\boldsymbol{p}_\gamma\, \boldsymbol{p}_Y\cdot\boldsymbol{\epsilon} + \mathcal{F}_8\, \boldsymbol{\sigma}\cdot\boldsymbol{p}_N\, \boldsymbol{p}_N\cdot\boldsymbol{\epsilon} + \mathcal{F}_9\, \boldsymbol{\sigma}\cdot\boldsymbol{p}_N\, \boldsymbol{p}_Y\cdot\boldsymbol{\epsilon} \\
& + \mathcal{F}_{12}\, \boldsymbol{\sigma}\cdot\boldsymbol{p}_Y\, \boldsymbol{p}_N\cdot\boldsymbol{\epsilon} + \mathcal{F}_{13}\, \boldsymbol{\sigma}\cdot\boldsymbol{p}_Y\, \boldsymbol{p}_Y\cdot\boldsymbol{\epsilon} + \mathcal{F}_{14}\, \boldsymbol{\sigma}\cdot\boldsymbol{\epsilon}\, \boldsymbol{\sigma}\cdot\boldsymbol{p}_\gamma \boldsymbol{\sigma}\cdot\boldsymbol{p}_N \\
& + \mathcal{F}_{15}\, \boldsymbol{\sigma}\cdot\boldsymbol{p}_Y\, \boldsymbol{\sigma}\cdot\boldsymbol{\epsilon} \boldsymbol{\sigma}\cdot\boldsymbol{p}_\gamma + \mathcal{F}_{16}\, \boldsymbol{\sigma}\cdot\boldsymbol{p}_Y\, \boldsymbol{\sigma}\cdot\boldsymbol{\epsilon} \boldsymbol{\sigma}\cdot\boldsymbol{p}_N + \mathcal{F}_{19}\, \boldsymbol{\sigma}\cdot\boldsymbol{p}_Y\, \boldsymbol{\sigma}\cdot\boldsymbol{p}_\gamma \boldsymbol{\sigma}\cdot\boldsymbol{p}_N\, \boldsymbol{p}_N\cdot\boldsymbol{\epsilon} \\
& + \mathcal{F}_{20}\, \boldsymbol{\sigma}\cdot\boldsymbol{p}_Y\, \boldsymbol{\sigma}\cdot\boldsymbol{p}_\gamma \boldsymbol{\sigma}\cdot\boldsymbol{p}_N\, \boldsymbol{p}_Y\cdot\boldsymbol{\epsilon} \Big] \;, \qquad (1)
\end{aligned}
$$

with m_N and m_Y are the nucleon and hyperon masses, E_N and E_Y their energies, $\boldsymbol{p}_\gamma$, $\boldsymbol{p}_N$ and $\boldsymbol{p}_Y$ the photon, nucleon and hyperon momenta and $\boldsymbol{\epsilon}$ the photon polarization. The amplitudes $\mathcal{F}_i$ are given in terms of kinematical quantities and amplitudes A_i which are related to the various tree diagrams. The rather lengthy expressions of $\mathcal{F}_i$ and A_i can be found in [19]. The operator can be rewritten in the form of

$$
t_{\gamma K} = i\,(\,L \,+\, i\boldsymbol{\sigma}\cdot\boldsymbol{K}\,) \;, \qquad (2)
$$

which is convenient for an application in the deuteron frame. However, in Eq. (2) both

spin-non-flip and spin-flip amplitudes L and $\boldsymbol{K}$ depend on the photon polarization $\boldsymbol{\epsilon}$ which complicates the calculation on the deuteron. To avoid this, we rewrite Eq. (1) in the form of

$$t_{\gamma K} \;=\; i\,(1, i\sigma_x, i\sigma_y, i\sigma_z) \begin{pmatrix} \mathcal{L}_x & \mathcal{L}_y & \mathcal{L}_z \\ \mathcal{K}_{xx} & \mathcal{K}_{xy} & \mathcal{K}_{xz} \\ \mathcal{K}_{yx} & \mathcal{K}_{yy} & \mathcal{K}_{yz} \\ \mathcal{K}_{zx} & \mathcal{K}_{zy} & \mathcal{K}_{zz} \end{pmatrix} \begin{pmatrix} \epsilon_x \\ \epsilon_y \\ \epsilon_z \end{pmatrix} \;. \tag{3}$$

Therefore, the elementary operator given by the 4×3 matrix in Eq. (3) becomes completely independent from the frame in which $\boldsymbol{\epsilon}$ and $\boldsymbol{\sigma}$ are defined. The expressions for the elements of this matrix read

$$\begin{aligned} \boldsymbol{\mathcal{L}} \;=\; & N \left[\mathcal{F}_{14}\, \boldsymbol{p}_\gamma \times \boldsymbol{p}_N + \mathcal{F}_{15}\, \boldsymbol{p}_\gamma \times \boldsymbol{p}_Y + \mathcal{F}_{16}\, \boldsymbol{p}_N \times \boldsymbol{p}_Y + \right. \\ & \left. \boldsymbol{p}_Y \cdot \boldsymbol{p}_\gamma \times \boldsymbol{p}_N \left(\mathcal{F}_{18}\, \boldsymbol{p}_\gamma + \mathcal{F}_{19}\, \boldsymbol{p}_N + \mathcal{F}_{20}\, \boldsymbol{p}_Y \right) \right] \end{aligned} \tag{4}$$

and

$$\mathcal{K}_{ij} \;=\; \delta_{ij}\, A + p_{\gamma,i}\, B_j + p_{N,i}\, C_j + p_{Y,i}\, D_j \;, \qquad i,j = x,y,z \;\;, \tag{5}$$

with

$$A \;=\; -N \left[\mathcal{F}_1 + \mathcal{F}_{14}\, \boldsymbol{p}_N \cdot \boldsymbol{p}_\gamma - \mathcal{F}_{15}\, \boldsymbol{p}_Y \cdot \boldsymbol{p}_\gamma - \mathcal{F}_{16}\, \boldsymbol{p}_N \cdot \boldsymbol{p}_Y \right] \;, \tag{6}$$

$$\boldsymbol{B} \;=\; -N \left[\left(\mathcal{F}_4 - \mathcal{F}_{14} - \mathcal{F}_{19}\, \boldsymbol{p}_N \cdot \boldsymbol{p}_Y \right) \boldsymbol{p}_N + \left(\mathcal{F}_5 + \mathcal{F}_{15} - \mathcal{F}_{20}\, \boldsymbol{p}_N \cdot \boldsymbol{p}_Y \right) \boldsymbol{p}_Y \right] \;, \tag{7}$$

$$\boldsymbol{C} \;=\; -N \left[\left(\mathcal{F}_8 + \mathcal{F}_{19}\, \boldsymbol{p}_Y \cdot \boldsymbol{p}_\gamma \right) \boldsymbol{p}_N + \left(\mathcal{F}_9 + \mathcal{F}_{16} + \mathcal{F}_{20}\, \boldsymbol{p}_Y \cdot \boldsymbol{p}_\gamma \right) \boldsymbol{p}_Y \right] \;, \tag{8}$$

$$\boldsymbol{D} \;=\; -N \left[\left(\mathcal{F}_{12} + \mathcal{F}_{16} + \mathcal{F}_{19}\, \boldsymbol{p}_N \cdot \boldsymbol{p}_\gamma \right) \boldsymbol{p}_N + \left(\mathcal{F}_{13} + \mathcal{F}_{20}\, \boldsymbol{p}_N \cdot \boldsymbol{p}_\gamma \right) \boldsymbol{p}_Y \right] \;. \tag{9}$$

Furthermore, we have

$$N = \left(\frac{E_N + m_N}{2m_N} \right)^{\frac{1}{2}} \left(\frac{E_Y + m_Y}{2m_Y} \right)^{\frac{1}{2}} \sqrt{\frac{m_Y}{E_Y}} \sqrt{\frac{m_N}{E_N}} \;. \tag{10}$$

III. CROSS SECTIONS AND POLARIZATION OBSERVABLES

As shown in Ref. [6], the cross section for the $\gamma + d \to K^+ + Y + N$ process in a general frame is expressed as

$$\begin{aligned} d\sigma(\mu_Y \nu_Y \mu_N \nu_N, \mu_d\, \epsilon) \;=\; & \frac{(2\pi)^3}{4 E_K E_\gamma} \int \frac{d\boldsymbol{p}_K}{(2\pi)^3} \frac{d\boldsymbol{p}_Y}{(2\pi)^3} \frac{d\boldsymbol{p}_N}{(2\pi)^3} \\ & \times \left| \sqrt{2} \langle\, \Psi^{(-)}_{\boldsymbol{q}_Y \mu_Y\, \nu_Y\, \mu_N\, \nu_N} \,|\, t_{\gamma K}(1) \,|\, \Psi_d\, \mu_d \,\rangle \right|^2 \\ & \times (2\pi)^4 \delta^{(4)}(P_d + Q - p_Y - p_N) \;, \end{aligned} \tag{11}$$

where the μ's and ν's denote spin and isospin magnetic quantum numbers and ϵ the photon polarization. The two-baryon final state state Ψ depends on $\boldsymbol{q}_Y$, the (nonrelativistic) relative momentum of the final hyperon and nucleon, while the momentum transfer to the final state is denoted by $\boldsymbol{Q} = \boldsymbol{p}_\gamma - \boldsymbol{p}_K$. The elementary operator $t_{\gamma K}(1)$ contains a label, indicating that it acts only on one of the baryons. The kinematics and the elementary operator are kept in their relativistic form, while nonrelativistic two-baryon wave functions are used.

In Ref. [6], we calculated cross sections in the total momentum zero frame of the final two baryons. However, the nuclear matrix element in Eq. (11) is not invariant under Lorentz transformations. The reason is the nonrelativistic treatment of the two baryons in the deuteron and the final state. Therefore, in the present paper we calculate all observables in the lab frame (the deuteron rest frame) which corresponds to the experimental situation.

The exclusive cross section is obtained by carrying out the integrations in Eq. (11) in the lab frame,

$$\begin{aligned} \frac{d\sigma}{dp_K d\Omega_K d\Omega_Y} &= \frac{\boldsymbol{p}_K^2}{(2\pi)^2\, 4E_\gamma E_K} \frac{m_Y m_N\, |\boldsymbol{p}_Y|}{|E_N + E_Y - E_Y \frac{\boldsymbol{Q}\cdot\boldsymbol{p}_Y}{p_Y^2}|} \\ &\quad \times \left| \sqrt{2}\, \langle\, \Psi^{(-)}_{\boldsymbol{q}_Y \mu_Y \nu_Y \mu_N \nu_N} \,|\, t_{\gamma K}(1) \,|\, \Psi_d \mu_d \,\rangle \right|^2 , \end{aligned} \tag{12}$$

where the relative momentum $\boldsymbol{q}_Y$ is determined by the nonrelativistic relation

$$\boldsymbol{q}_Y = \boldsymbol{p}_Y - \frac{m_Y}{m_Y + m_N} \boldsymbol{Q} \ . \tag{13}$$

The calculations of the nuclear matrix element are discussed in detail in Ref. [6], but Eqs. (3.13), (3.14) and (3.15) therein should be replaced by the expressions in the lab frame,

$$\boldsymbol{k}_Y = \boldsymbol{q}_Y + \frac{m_Y}{m_Y + m_N} \boldsymbol{Q} \ , \tag{14}$$

$$\boldsymbol{k}_1 = \boldsymbol{q}_Y - \frac{m_N}{m_Y + m_N} \boldsymbol{Q} \ , \tag{15}$$

$$\boldsymbol{q} = \boldsymbol{q}_Y - \frac{m_N}{m_Y + m_N} \boldsymbol{Q} \ . \tag{16}$$

The inclusive ^{2}H(γ, K^+) cross section can be obtained by integrating Eq. (12) over Ω_Y. However, this turns out to be inconvenient since the integration limits over Ω_Y are complicated and, secondly, the phase space factor appearing in Eq. (12) can become singular. We

therefore take as the integration variable the direction of the hyperon momentum $\boldsymbol{p}_Y^{\rm cm}$ in the c.m. frame of the final two baryons.

Thus, the inclusive cross section (in the lab frame) is expressed as

$$\begin{aligned}\frac{d\sigma}{dp_K d\Omega_K} &= \frac{\boldsymbol{p}_K^2}{(2\pi)^2\, 4E_\gamma E_K W}\sum_Y m_Y m_N\, |\boldsymbol{p}_Y^{\rm cm}| \\ &\times\frac{1}{6}\sum_{\mu_d\,\epsilon}\sum_{\mu_Y\,\mu_N}\sum_{\nu_Y\,\nu_N}\int d\hat{\boldsymbol{p}}_Y^{\rm cm}\left|\sqrt{2}\,\langle\,\Psi^{(-)}_{\boldsymbol{q}_Y\mu_Y\nu_Y\mu_N\nu_N}\,|\,t_{\gamma K}(1)\,|\,\Psi_d\mu_d\,\rangle\right|^2\,, \qquad (17)\end{aligned}$$

where $W^2=(P_d+Q)^2$.

In addition to the inclusive ${}^2{\rm H}(\gamma,K^+)$ and exclusive ${}^2{\rm H}(\gamma,K^+Y)$ cross sections, we calculate the hyperon recoil polarization P_y, the beam polarization asymmetry Σ and the double polarizations C_x, C_z which are given by

$$P_y = \frac{{\rm Tr}\{MM^+\sigma_y\}}{{\rm Tr}\{MM^+\}}, \qquad (18)$$

$$\Sigma = \frac{{\rm Tr}\{M_{\epsilon=\epsilon_y}M^+_{\epsilon=\epsilon_y}\}-{\rm Tr}\{M_{\epsilon=\epsilon_x}M^+_{\epsilon=\epsilon_x}\}}{{\rm Tr}\{M_{\epsilon=\epsilon_y}M^+_{\epsilon=\epsilon_y}\}+{\rm Tr}\{M_{\epsilon=\epsilon_x}M^+_{\epsilon=\epsilon_x}\}}, \qquad (19)$$

$$C_x = \frac{{\rm Tr}\{M_{\epsilon=\epsilon_1}M^+_{\epsilon=\epsilon_1}\sigma_x\}}{{\rm Tr}\{M_{\epsilon=\epsilon_1}M^+_{\epsilon=\epsilon_1}\}}, \qquad (20)$$

$$C_z = \frac{{\rm Tr}\{M_{\epsilon=\epsilon_1}M^+_{\epsilon=\epsilon_1}\sigma_z\}}{{\rm Tr}\{M_{\epsilon=\epsilon_1}M^+_{\epsilon=\epsilon_1}\}}. \qquad (21)$$

In the definitions above, M is the K^+YN break-up amplitude

$$M(\mu_Y\,\mu_N\,;\mu_d\,\epsilon)=\langle\,\Psi^{(-)}_{\boldsymbol{q}_Y\mu_Y\,\nu_Y\,\mu_N\,\nu_N}\,|\,t_{\gamma K}(1)\,|\,\Psi_d\,\mu_d\,\rangle \qquad (22)$$

with $M_{\epsilon=\epsilon_y}$ as the amplitude where the photon polarization points into the y-axis, $\boldsymbol{\epsilon}=\boldsymbol{\epsilon}_y$, and so on. The photon polarization $\boldsymbol{\epsilon}_1=-\frac{1}{\sqrt{2}}(\boldsymbol{\epsilon}_x+i\boldsymbol{\epsilon}_y)$ describes the helicity state $+1$. The beam polarization asymmetry Σ is obtained with linearly polarized photon, while the double polarization observables C_x and C_z are the hyperon polarization along with circularly polarized photons.

IV. RESULTS AND DISCUSSIONS

As mentioned in Sec. I, the aim of this paper is twofold, i.e., to study the YN final-state interaction (FSI) effects as well as to extract the information on the elementary amplitude in the region where FSI effects are negligible. For this purpose, we limit the outgoing kaon lab angles to the forward ones less than 20° because we expect other types of FSI would start to show some effects for larger kaon angles. As a sample, the incoming photon energy of 1.3 GeV is chosen throughout this paper. We analyze observables for two YN forces, i.e., NSC89 [20] and NSC97f [21], both of which give the correct hypertriton binding energy [22]. The NSC89 interaction is a soft-core one-boson-exchange model based on Regge-pole theory, and a straightforward extension of the NN model through the application of SU(3). The NSC97f model is an improvement of NSC89. Reference [21] gives the six models from NSC97a through NSC97f classified by the different choices for the magnetic vector-meson $F/(F+D)$ ratio, which results in a different balance between ${}^1S_0$ and ${}^3S_1$ ΛN scattering lengths. Among them only the two models, NSC89 and NSC97f, reproduce the hypertriton binding energy, but still have different S-wave scattering lengths [22, 23]. A rigorous four-body calculation [24] has also shown that both of these two can not reproduce the bound states of ${}^4_\Lambda$H and ${}^4_\Lambda$He. Thus, the present analysis is expected to supply additional information on the YN interaction via the continuum.

The deuteron wave function is generated by the Nijmegen93 potential [25]. Some figures and discussions for the inclusive observables are similar to those which are already given in the previous paper [6], but we include them for the convenience of the readers. Notice that we present all observables in the deuteron rest frame as mentioned in Sec. III, which differs from the former paper.

A. Inclusive observables

First, inclusive cross sections for the kaon lab angle $\theta_K = 1°$ are shown in Fig. 1 as a function of the kaon lab momentum p_K. The individual contributions of the Λn, $\Sigma^0 n$ and $\Sigma^- p$ processes are shown separately and summed up. The YN final-state interaction NSC97f is used. The two pronounced peaks are seen around $p_K = 950$ and $p_K = 810$ MeV/c. These p_K values correspond to the quasifree scattering (QFS) condition where one of the nucleons in

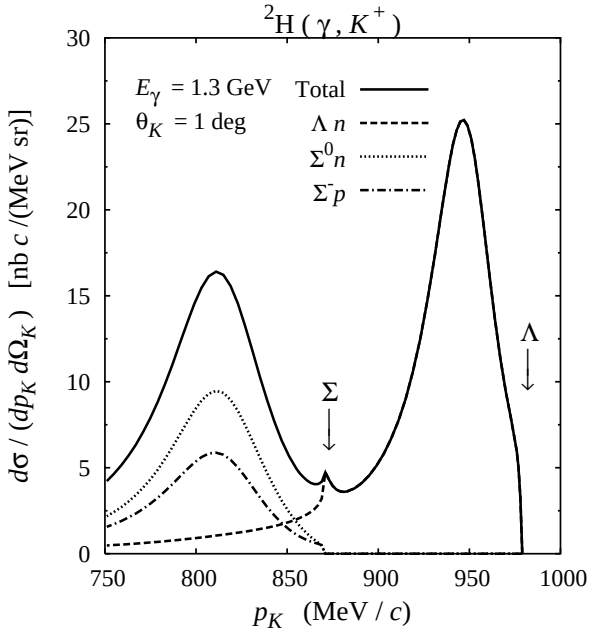

FIG. 1: Inclusive $^2\mathrm{H}(\gamma, K^+)$ cross section as a function of kaon lab momentum p_K for kaon lab angle $\theta_K = 1^\circ$ and photon beam energy $E_\gamma = 1.3$ GeV. The NSC97f potential is used for the YN sector. The contributions from the Λn, $\Sigma^0 n$ and $\Sigma^- p$ processes are shown separately and summed up. The arrows indicate the ΛN and ΣN thresholds.

the deuteron sits as a spectator and has zero momentum. In Fig. 2, the inclusive cross sections are compared with the result obtained by using the plane wave impulse approximation (PWIA) and the result generated by the other YN interaction NSC89. The two peaks are dominated by the PWIA contribution but some FSI effects can be seen especially around $p_K = 810$ MeV/c, about which we will also discuss in the next subsection. In Fig. 2 we also see the FSI effects around the ΛN and the ΣN thresholds. Around the ΣN threshold, the NSC97f result shows a prominent cusp-like structure, whereas the NSC89 one displays only a little deviation from the PWIA result. This fact can be traced back to the location of the S-matrix pole for the ΛN-ΣN system around the ΣN threshold, the full detail of which has been discussed in Refs. [6] and [26]. The structure produced by NSC97f with different ΛN-ΣN partial wave contributions is enlarged in Fig. 3. The line indicated by $J_{\max} = 0$ incorporates the $^1S_0$ and $^3P_0$ components and $J_{\max} = 1$ includes all the partial waves up to $J = 1$. It shows that the $J = 1$ state is responsible for this structure, which is consistent with the known fact that the S-matrix pole mentioned above exists in the $^3S_1$-$^3D_1$ state.

In Fig. 4, the inclusive cross sections for three different kaon lab angles, i.e., $\theta_K = 1^\circ, 10^\circ$

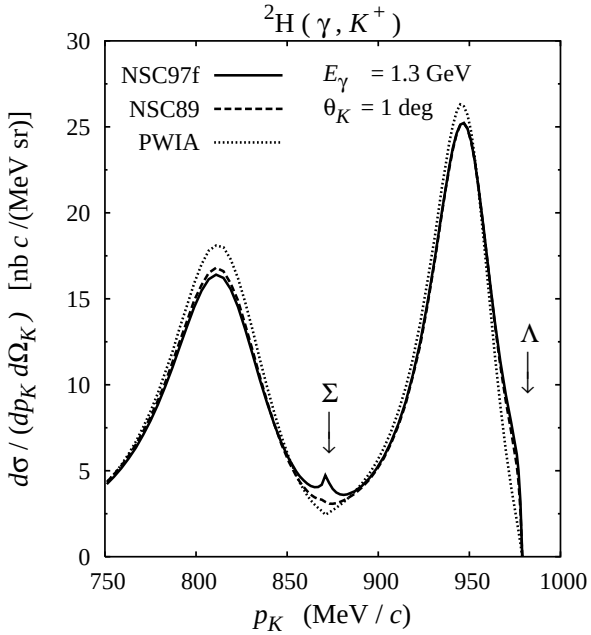

FIG. 2: Inclusive $^2\mathrm{H}(\gamma, K^+)$ cross section as a function of kaon lab momentum p_K for kaon lab angle $\theta_K = 1^\circ$ and photon beam energy $E_\gamma = 1.3$ GeV. The PWIA result is compared to the two YN force predictions. The FSI effects are pronounced near the ΛN and ΣN thresholds (indicated by the arrows) as well as on top of the two peaks.

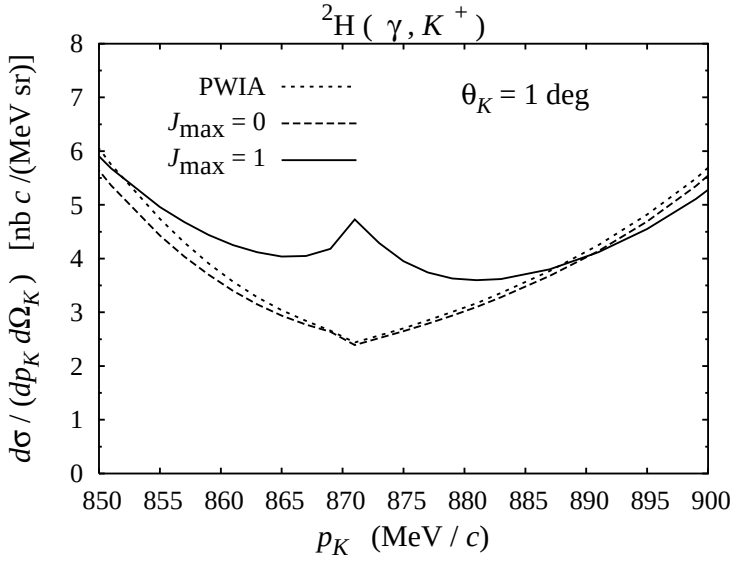

FIG. 3: The results in Fig. 2 for NSC97f and PWIA enlarged around the ΣN threshold. The individual contributions of ΛN-ΣN partial waves are also shown.

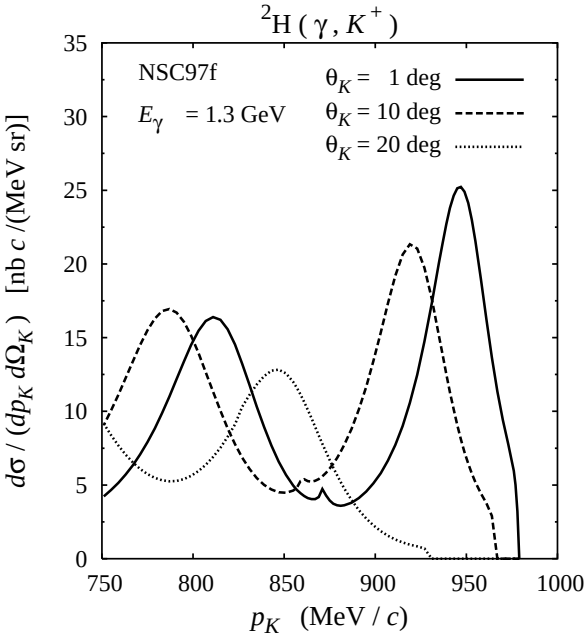

FIG. 4: Inclusive $^2\mathrm{H}(\gamma, K^+)$ cross section as a function of the kaon lab momentum p_K for kaon lab angles $\theta_K = 1^\circ, 10^\circ$ and 20° and photon beam energy $E_\gamma = 1.3$ GeV. The YN interaction NSC97f has been used to obtain these results.

and 20° are shown, where the cross section maxima shift as the kaon angle increases. We confirmed that, in contrast to the $\theta_K = 1^\circ$ case, the cross sections at $\theta_K = 20^\circ$ have little YN FSI effects in the region of p_K larger than 750 MeV/c. Also we verified that the $J_{\max} = 1$ results are converged with regard to the angular momentum decomposition of the YN system throughout the figures for the inclusive cross sections.

Finally, in Fig. 5 we give the three-dimensional plots of the inclusive cross sections as a function of lab kaon momentum p_K and angle θ_K, where individual contributions of the Λn, $\Sigma^0 n$ and $\Sigma^- p$ processes are also shown. On the plane of $p_K = 750 \sim 1000$ MeV/c and $\theta_K = 1 \sim 20^\circ$, we can identify the area where the cross sections are large. In particular, the two peaks seen in Fig. 1 form two ridges in the $p_K - \theta_K$ plane, and it is confirmed that these ridges run along the $p_K - \theta_K$ values which satisfy the QFS condition.

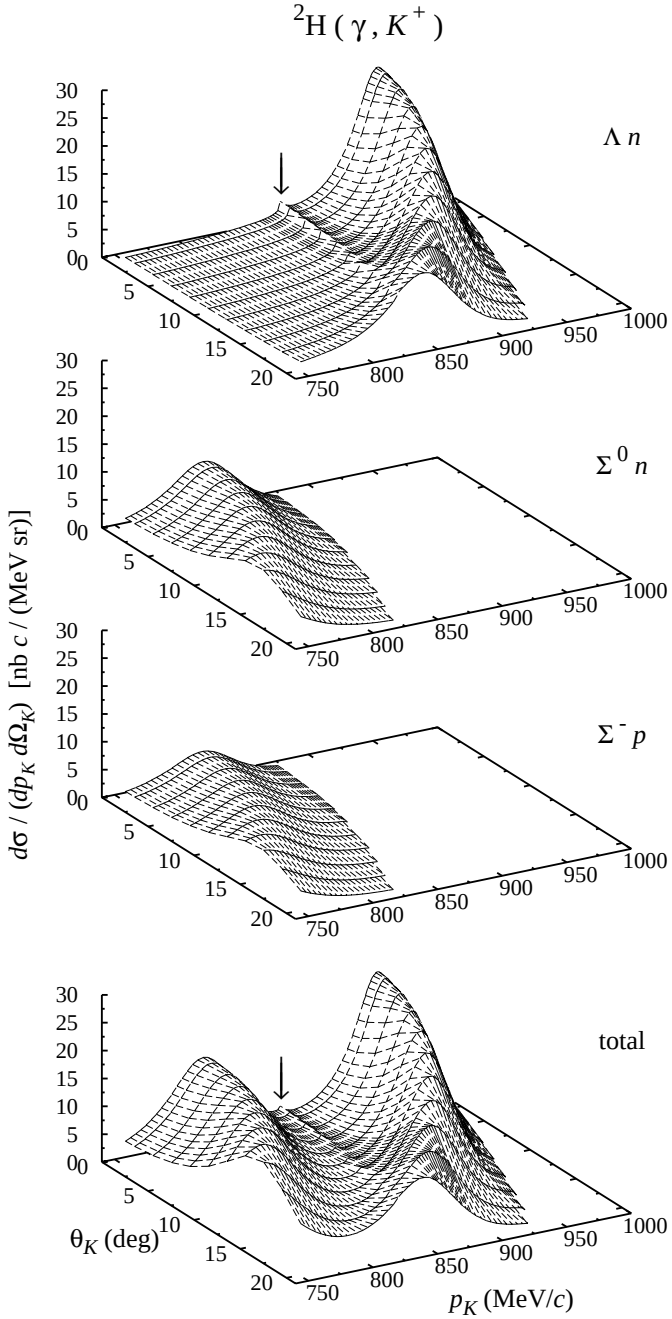

FIG. 5: Inclusive $^2\mathrm{H}(\gamma, K^+)$ cross section as a function of kaon lab momentum p_K and angle θ_K for photon beam energy $E_\gamma = 1.3$ GeV. The NSC97f YN interaction is used. The contributions from the Λn, $\Sigma^0 n$ and $\Sigma^- p$ processes are shown separately and summed up. The arrows indicate the ΣN threshold.

B. Exclusive observables

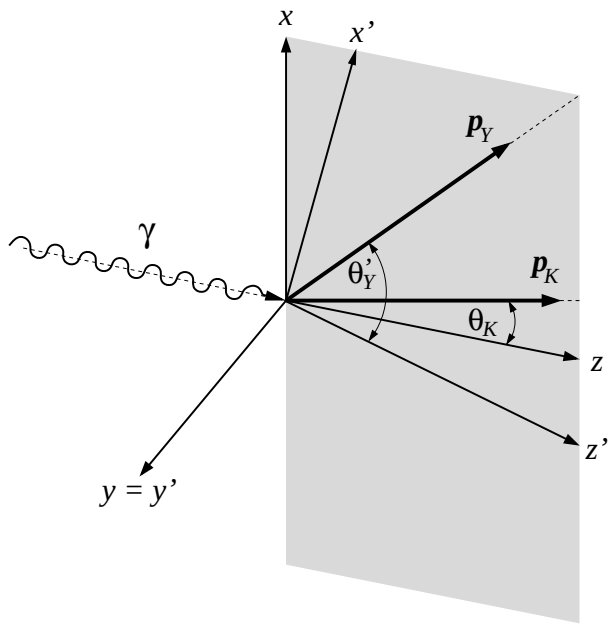

FIG. 6: Kinematics in the deuteron rest frame. The z axis points into the photon beam direction $\boldsymbol{p}_\gamma$ and the kaon lies in the x-z plane. The momentum transferred to the YN system, $\boldsymbol{p}_\gamma - \boldsymbol{p}_K$, defines the z' axis. The hyperon angle θ'_Y is measured from the z' axis.

There are many ways to present exclusive observables including the polarization ones. Here, we show five observables, i.e., differential cross section $d\sigma/dp_K d\Omega_K d\Omega_Y$, hyperon polarization P_y, double polarizations C_z and C_x, and the beam polarization asymmetry Σ, as a function of the hyperon angle for fixed kaon momentum and kaon angle. As kaon momenta, we select $p_K = 975$ MeV/c (just above the Λn threshold), 944 MeV/c (close to the Λ QFS peak), 870 and 860 MeV/c (near the ΣN threshold), and 810 MeV/c (on the Σ QFS peak).

In Fig. 6, an illustration of the kinematics is given. The z axis points into the photon beam direction and the kaon lies in the x-z plane, as usual. However, for the outgoing YN system, Li and Wright [27] found a characteristic axis, which corresponds to the direction of the momentum transfer $\boldsymbol{p}_\gamma - \boldsymbol{p}_K$ to the YN system and defines the z' axis as shown in Fig. 6. Thus a new coordinate system x'-y-z' is introduced with the x' axis defined by $\hat{\boldsymbol{e}}_y \times \hat{\boldsymbol{e}}_{z'}$. We use this primed coordinate system as the reference system for the hyperon angles, which are denoted by θ'_Y and ϕ'_Y. The hyperon polarization is defined with respect to the ordinary x-y-z system. For all results given below, we take $\phi'_Y = 0$ and the hyperon is on the x'-z'

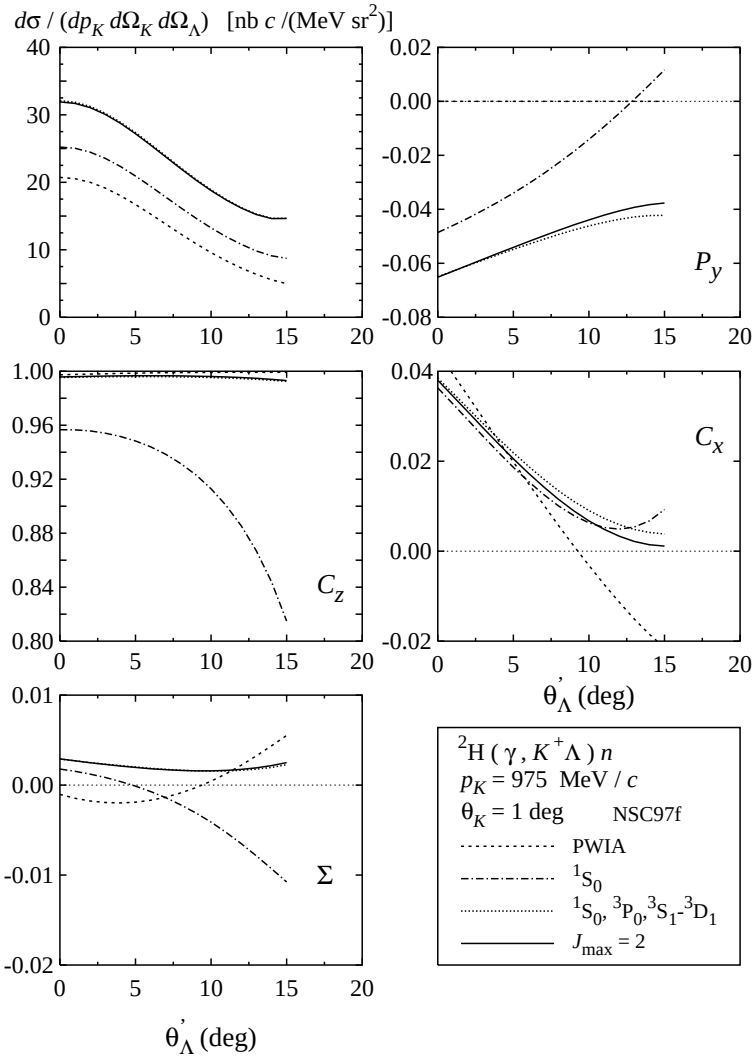

FIG. 7: Differential cross section and polarization observables P_y, C_z, C_x and Σ, for the ^{2}H$(\gamma, K^+\Lambda)n$ process as a function of the hyperon lab angle θ'_Λ. The kaon lab momentum and angle are fixed at $p_k = 975$ MeV/c and $\theta_K = 1^\circ$. The YN interaction NSC97f is used and different partial wave contributions are shown. The possible Λ angles are limited to less than 17°.

(and x-z) plane.

Now, in Fig. 7 the five observables in the ^{2}H$(\gamma, K^+\Lambda)n$ process are shown as a function of θ'_Λ for $p_k = 975$ MeV/c just above the Λn threshold. Here PWIA is compared with the FSI results obtained by the NSC97f YN interaction. The dominant YN partial wave contributions are also shown. The line indicated by $J_{\rm max} = 2$ incorporates all the partial wave up to $J = 2$, and gives the converged results. The differential cross sections clearly indicate FSI effects starting from $\theta'_\Lambda = 0^\circ$ to which $^1S_0$ and $^3S_1$-$^3D_1$ force components

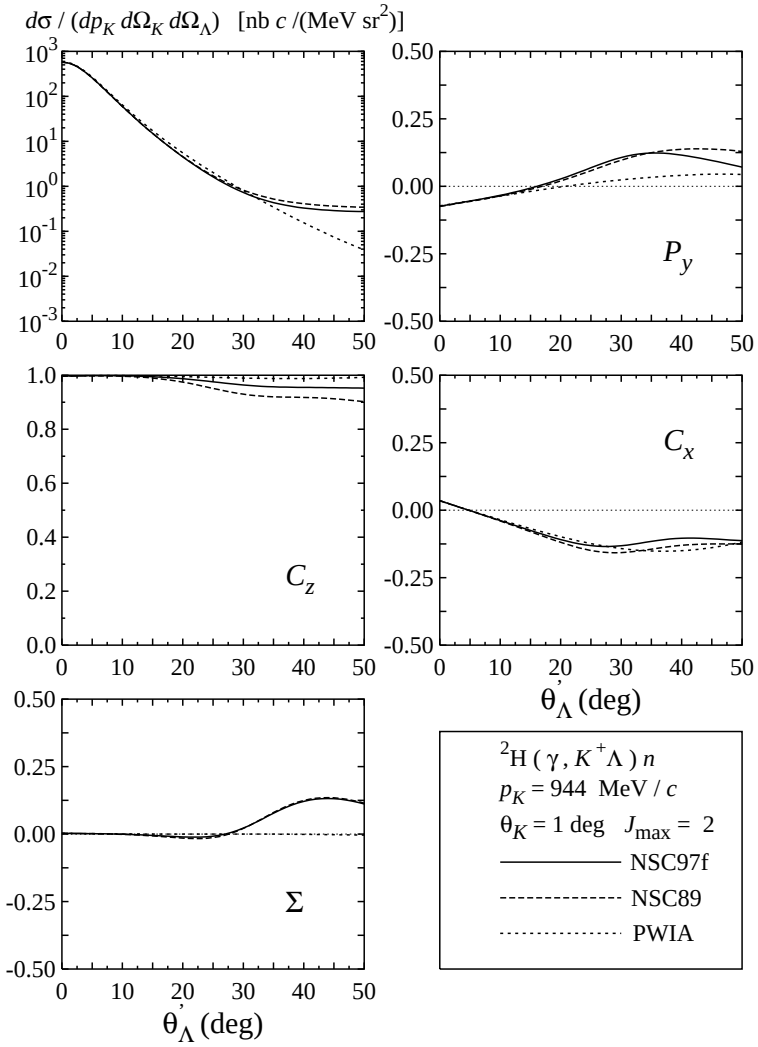

FIG. 8: Same as Fig. 7, but for kaon lab momentum $p_k = 944$ MeV/c. The results obtained from NSC97f and NSC89 are compared with the one from PWIA.

contribute. In the double polarization C_z, $^1S_0$ shows a visible effect but the inclusion of the $^3S_1$ cancels it and shifts it on the same line as PWIA. Please note, for the sake of better visibility of the effects we change the scales in various panels in Fig. 7 and the following ones.

Figure 8 shows the results for $p_K = 944$ MeV/c which is close to one of the peak positions in Fig. 2 (inclusive cross section). The FSI effects for NSC97f and NSC89 are compared with PWIA. In the forward peak of the differential cross sections, PWIA dominates up to $\theta'_\Lambda = 30^\circ$ which forms the dominant part of the Λ QFS peak in Fig. 2. (To be precise, the QFS condition corresponds to $\theta_K = 1.6^\circ$ and $\theta'_\Lambda = 0$ at this p_K value.) However, FSI still

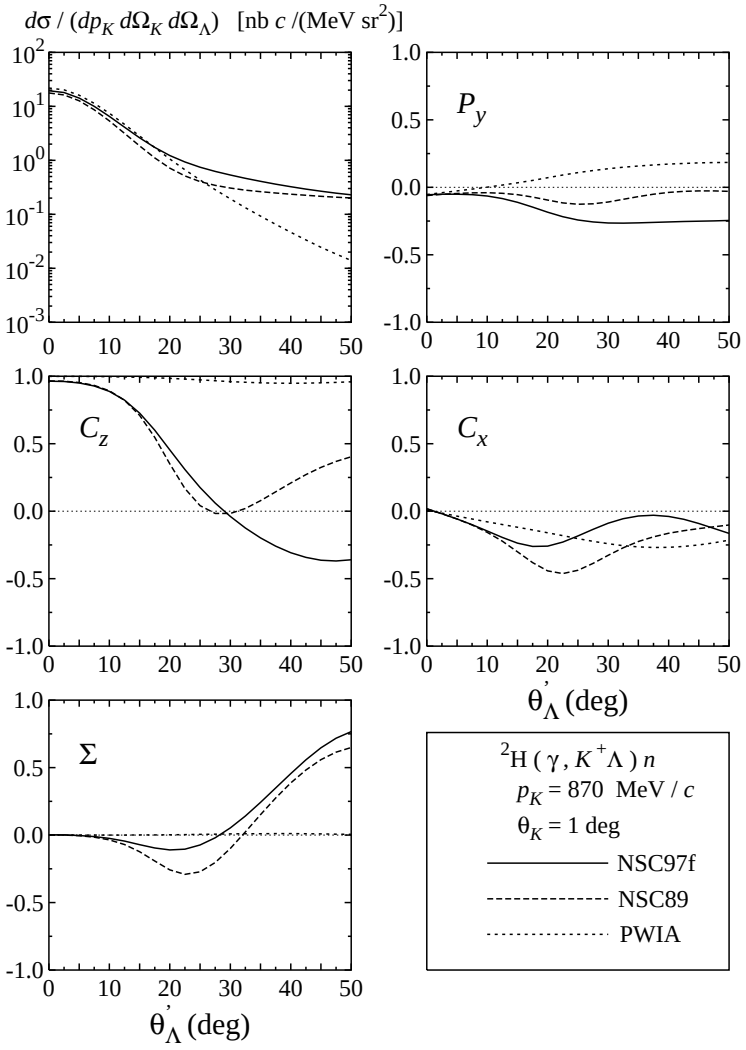

FIG. 9: Differential cross section and polarization observables P_y, C_z, C_x and Σ for the ^{2}H$(\gamma, K^+\Lambda)n$ process as functions of Λ angle θ'_Λ. The kaon lab momentum and angle are fixed at $p_k = 870$ MeV/c and $\theta_K = 1^\circ$. The results by the YN interactions NSC97f and NSC89 are compared with that by PWIA.

shows some effects above $\theta'_\Lambda = 30^\circ$. The NSC97f and NSC89 interactions give almost the same effects except for C_z.

Next, the results of ^{2}H$(\gamma, K^+\Lambda)n$ for p_K=870 MeV/c and $\theta_K = 1^\circ$ which is very close to the ΣN threshold are shown in Figs. 9 and 10. Figure 10 exhibits the dominant partial wave contributions in NSC97f. Because of the closeness to the threshold, the differential cross sections show a rather flat behavior and FSI effects are significant. In particular, the double polarization C_z with FSI deviates from PWIA even at $\theta'_\Lambda = 0^\circ$ and drastically

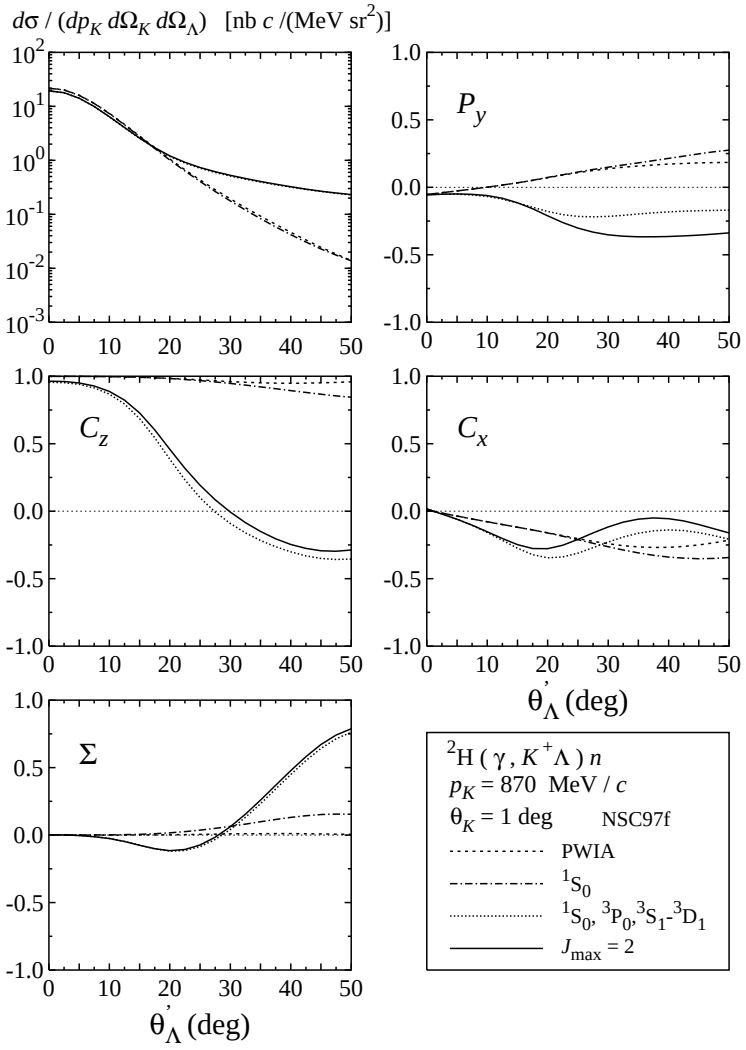

FIG. 10: Same as Fig. 9, but the YN interaction NSC97f is used and different partial wave contributions are shown.

above $\theta'_\Lambda = 20°$. Also NSC97f and NSC89 are clearly distinct from each other in this case. Figure 10 reveals the fact that these effects come from ΛN-ΣN $^3S_1$-$^3D_1$ component which is expected from the t-matrix pole existence in this partial wave as mentioned in the previous subsection.

We also show the results for p_K=870 MeV/c but for a larger kaon angle $\theta_K = 17°$ in Fig. 11. This case is rather far from the ΣN threshold, and shows the forward-peak cross sections, but prominent FSI effects are still seen in P_y above $\theta'_\Lambda = 20°$.

Now, let us give the results for the $\Sigma^- p$ and $\Sigma^0 n$ exit channels. Figures 12 ($\Sigma^- p$) and 13 ($\Sigma^0 n$) show the observables for $p_K = 860$ MeV/c and $\theta_K = 1°$, which is still close to the ΣN

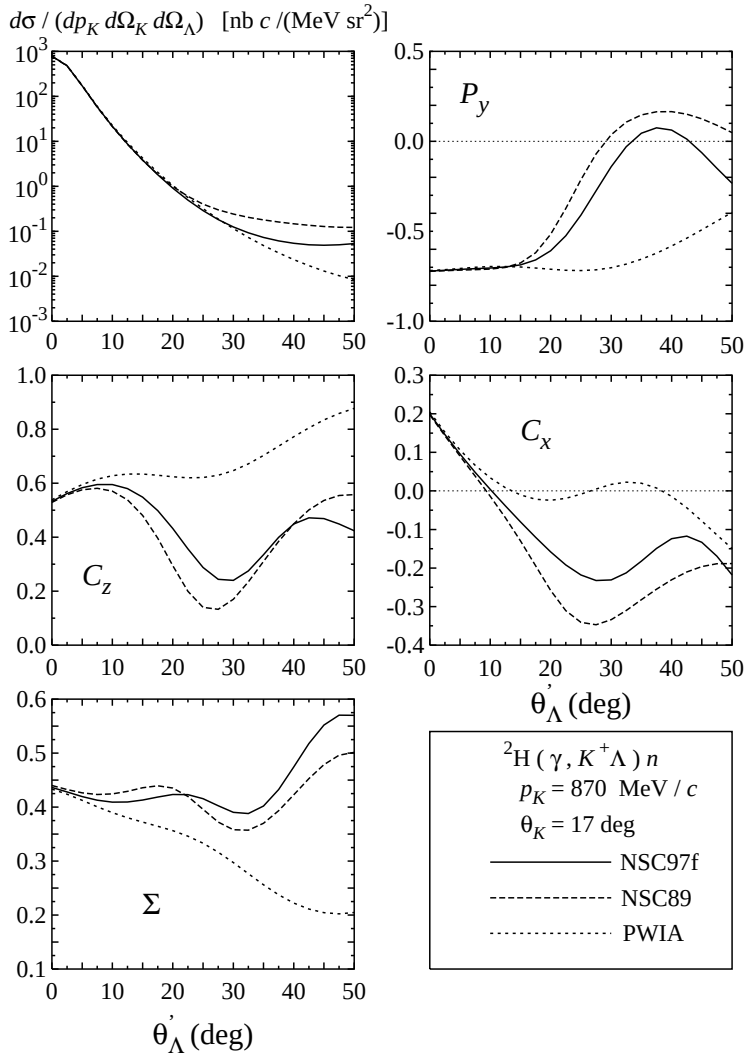

FIG. 11: Same as Fig. 9, but for kaon lab angle $\theta_K = 17°$.

threshold, and the available lab angles of the hyperon θ'_Σ are limited to less than 21°. As in Fig. 10, FSI effects are prominent. The $\Sigma^- p$ channel gives more visible FSI effects than $\Sigma^0 n$, where both of the $\frac{1}{2}$ and $\frac{3}{2}$ ΣN isospin components are included. Not only the $^3S_1$-$^3D_1$, but also $^1S_0$ contributions can be seen, especially in C_z.

The results for $p_K = 810$ MeV/c and $\theta_K = 1°$ which corresponds to the Σ QFS peak position in Fig. 2 are given in Fig. 14 ($\Sigma^- p$ channel) and in Fig. 15 ($\Sigma^0 n$ channel). In contrast to the case for $p_K = 944$ MeV/c (Λ QFS), most observables show significant FSI effects starting from θ'_Σ less than 20°. This is the reason why fairly large FSI effects are seen on the top of the Σ QFS peak around $p_K = 810$ MeV/c in Fig. 2.

In Fig. 16, the three-dimensional plots of the five observables as functions of kaon lab

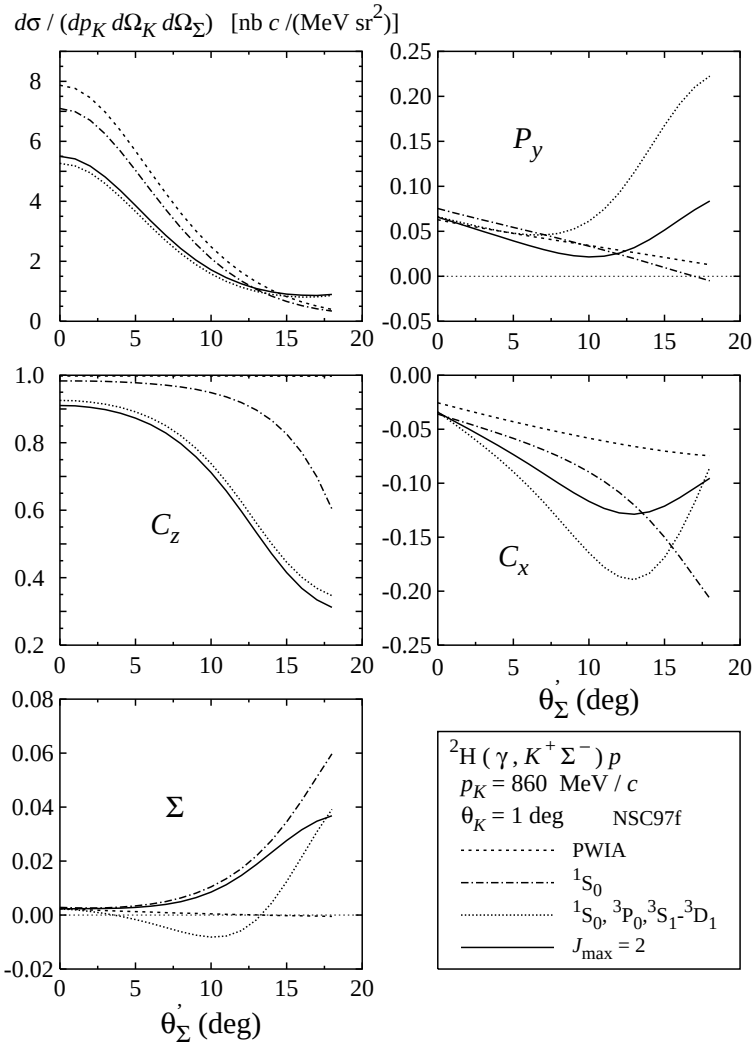

FIG. 12: Differential cross section and polarization observables P_y, C_z, C_x and Σ for the ^{2}H$(\gamma, K^+\Sigma^-)p$ process as functions of the Σ angle θ'_Σ. The kaon lab momentum and angle are fixed at $p_k = 860$ MeV/c and $\theta_K = 1^\circ$. The YN interaction NSC97f is used and different partial wave contributions are shown. The available Σ lab angles are limited to less than $\theta'_\Sigma = 21^\circ$.

momentum p_k and angle θ_K are given for the ^{2}H$(\gamma, K^+\Lambda)n$ as an example. The hyperon lab angle is fixed at the forward angle $\theta'_Y = 5^\circ$. As in the inclusive case (Fig. 5) we give the information on the θ_K dependence of the observables over the range of θ_K less than 30°.

Before closing this section, we would like to discuss the influence from other rescattering processes which are not included in the present analysis. As mentioned in Sec. I, Refs. [7] and [8] have evaluated some of those rescattering contributions. The former incorporates several two-body kaon production mechanisms, and the latter includes the pion mediated

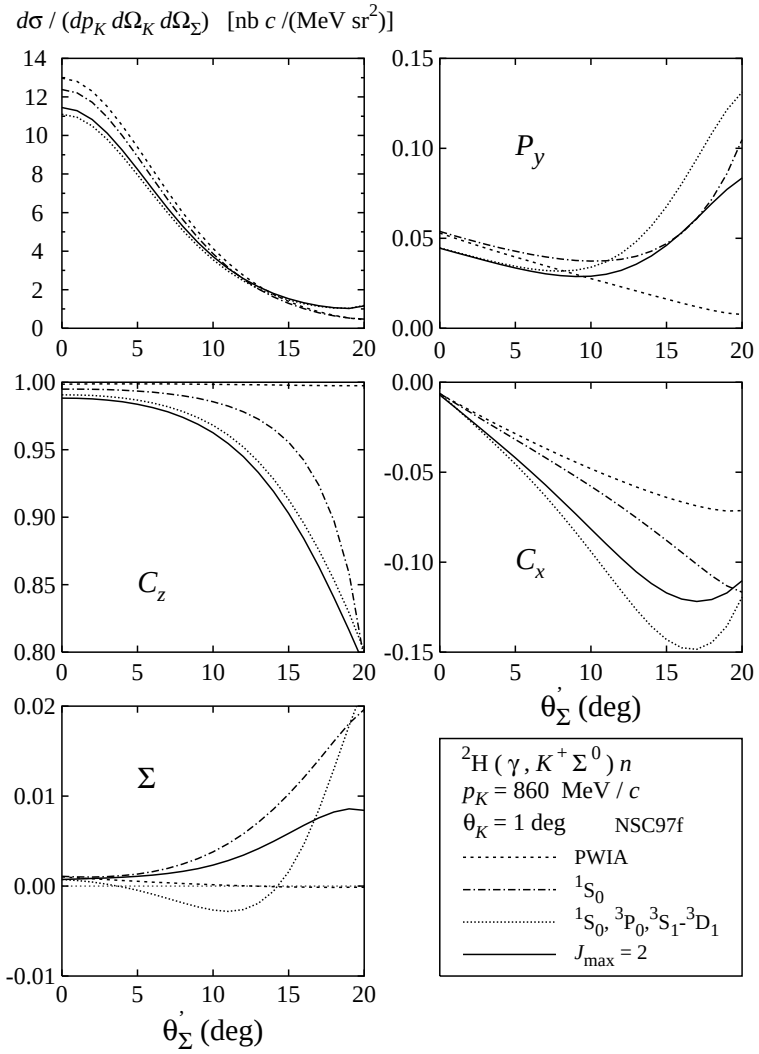

FIG. 13: Same as Fig. 12, but for the ^{2}H$(\gamma, K^+\Sigma^0)n$ process.

process $\gamma d \to \pi NN \to KYN$ in addition to the YN and KN rescattering. In considering the effects of these rescattering processes, we stress that the present analysis focuses on a restricted kinematical region where the kaon is scattered forward with large momentum and small relative energy is distributed between the hyperon and the nucleon.

In Fig. 8 ($p_K = 944$ MeV/c, $\theta_K = 1^\circ$), T_K(kinetic energy of the kaon) is 572 MeV, but $T_{\Lambda-N}$(relative energy between Λ and N) is 25 MeV. The QFS condition further determines the Λ scattering angle $\theta'_\Lambda = 0$ ($\theta_\Lambda = 1.6^\circ$) where T_Λ(Λ kinetic energy)= 56 MeV and $T_N = 0$. The extreme cases are given by Figs. 12 and 13, which are close to the ΣN threshold and $T_{\Sigma-N}$ is only 7 MeV, while $T_K = 498$ MeV.

In contrast to this, Ref. [7] supposes a large relative energy between Y and N in the

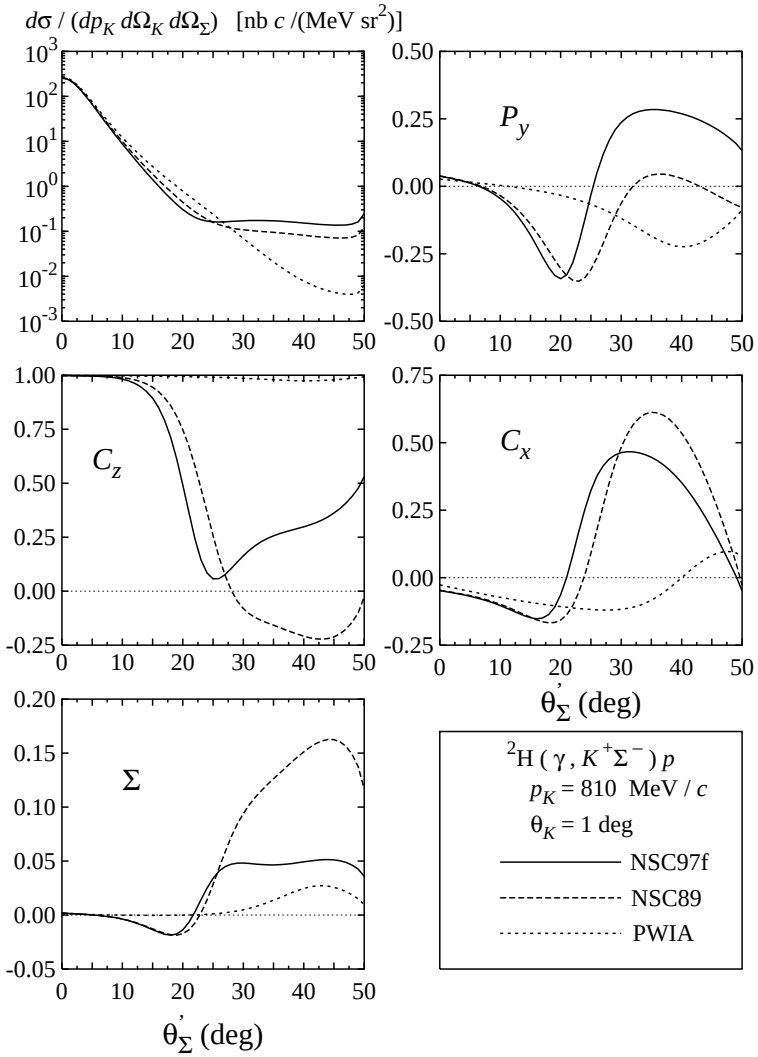

FIG. 14: Differential cross section and polarization observables P_y, C_z, C_x and Σ for the ^{2}H$(\gamma, K^+\Sigma^-)p$ process as functions of the Σ angle θ'_Σ. The kaon lab momentum and angle are fixed at $p_k = 810$ MeV/c and $\theta_K = 1°$. The results by the YN interactions NSC97f and NSC89 are compared with that by PWIA.

final state, for example, Fig. 7 of Ref. [7] shows the case of $E_\gamma = 1500$ MeV, $\theta_K = 15°$, and $T_K = 500$ (or 200) MeV, where $T_{\Lambda-N}$ amounts to 221 (419) MeV. Thus the YN relative energies in the present work are at least 10 times smaller than in Ref. [7].

Reference [8] focuses on the effects of the pion mediated process, giving the total cross sections and the semi-inclusive results where the contributions from various p_K are integrated. Recently, the same method has been applied in Ref. [28] to the exclusive cross sections for just the same final states as in Fig. 9 (p_K=870 MeV/c), as well as Figs. 14

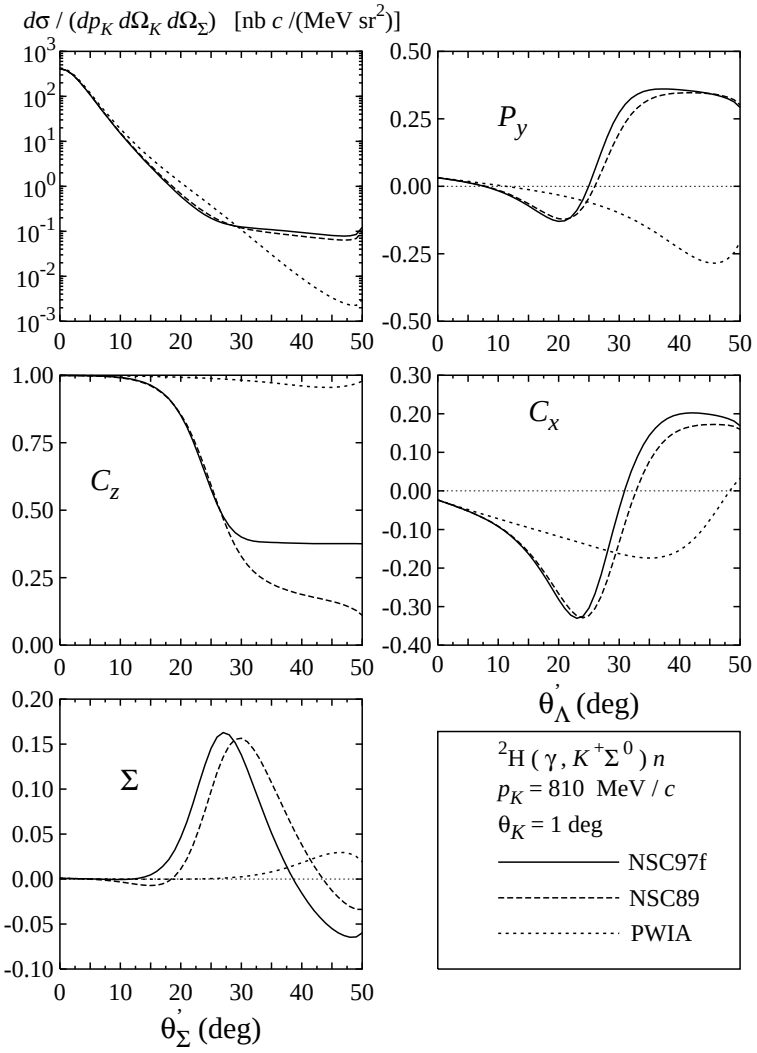

FIG. 15: Same as Fig. 14, but for the $^2\mathrm{H}(\gamma, K^+\Sigma^0)n$ process.

and 15 ($p_K = 810\mathrm{MeV}/c$). Important is to note that no visible effect of the pion mediated process is seen. The effects of this process appear at small p_K values such as 400 MeV/c in the inclusive cross sections for $E_\gamma = 1140$ MeV.

From all the facts mentioned above, we conclude that in the kinematical region where the present analysis concentrates, either QFS or YN FSI is expected.

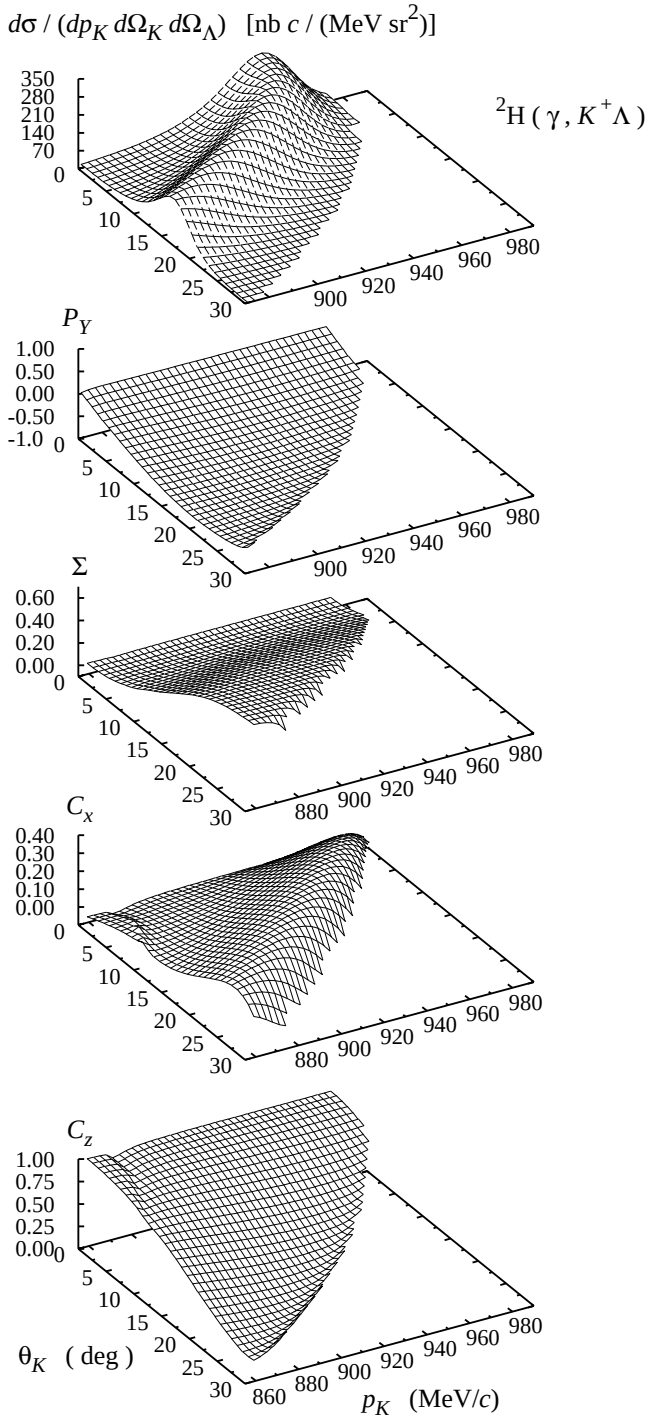

FIG. 16: Three-dimensional plots of exclusive observables $d\sigma/dp_K d\Omega_K d\Omega_\Lambda$, P_y, Σ, C_x and C_z. for the $^2\mathrm{H}(\gamma, K^+\Lambda)n$ process as functions of kaon lab momentum p_k and lab angle θ_K. The Λ lab angle is fixed at $\theta'_\Lambda = 5^\circ$.

V. SUMMARY AND CONCLUSION

We have evaluated single and double polarization observables as well as the inclusive and exclusive cross sections for the $\gamma + d \to K^+ + Y + N$ reactions at $E_\gamma = 1.3$ GeV, which are immediately accessible experimentally by electron beam facilities such as JLab and SPring8. An updated photoproduction operator for the $\gamma + N \to K^+ + Y$ process and modern hyperon-nucleon forces, NSC89 and NSC97f are used. The kinematical region of the kaon scattered forward with large momentum is thoroughly investigated where either the quasifree scattering or the YN final-state interaction is expected. The quasifree scattering is found to generate large cross sections and to form the ridges on the $p_K - \theta_K$ plane where one could extract the information on the elementary kaon photoproduction processes. The YN final-state interaction effects are significant, especially around the ΛN and ΣN thresholds. Around the ΛN thresholds, both of the $^1S_0$ and $^3S_1$ YN force components show the effects, while around the ΣN thresholds, $^3S_1$-$^3D_1$ gives the main contribution. In the latter case the two YN forces give quite different predictions, reflecting the different structure. The polarization observables, in particular the double polarization C_z, are sensitive to the final-state interaction effects. Precise data would help to clarify the property of the ΛN-ΣN interaction and also help to extract the elementary amplitude from the quasifree scattering region.

Acknowledgments

K.M. thanks the few-body group of the Ruhr University Bochum for the kind hospitality during his stay. T.M. thanks the Okayama University of Science for the hospitality extended to him during his stay in Okayama and the support from the Faculty of Mathematics and Sciences as well as from the Hibah Pascasarjana. This work was supported by "Academic Frontier" Project for Private Universities: matching fund subsidy from MEXT (Ministry of Education, Culture, Sports, Science and Technology), Japan.

---

[1] R.A. Adelseck and L.E. Wright, Phys. Rev. C **39**, 580 (1989); X. Li and L.E. Wright, J. Phys. G: Nucl. Part. Phys. **17**, 1127 (1991); S.R. Cotanch and S. Hsiao, Nucl. Phys. **A450**, 419c

(1986).

[2] T. Mart, C. Bennhold, and C. Hyde-Wright, Phys. Rev. C **51** R1074 (1995).

[3] J. C. David, C. Fayard, G. H. Lamot, and B. Saghai, Phys. Rev. C **53**, 2613 (1996).

[4] X. D. Li, L. E. Wright and C. Bennhold, Phys. Rev. C **45**, 2011 (1992).

[5] O. Hashimoto, private communication.

[6] H. Yamamura, K. Miyagawa, T. Mart, C. Bennhold, H. Haberzettl, and W. Glöckle, Phys. Rev. C **61**, 014001 (2000).

[7] O. V. Maxwell, Phys. Rev. C **69**, 034605 (2004).

[8] A. Salam and H. Arenhoevel, Phys. Rev. C **70**, 044008 (2004).

[9] JLab completed experiment, E-89-045, *Study of kaon photoproduction on deuterium* (B. Mecking, spokesperson).

[10] JLab completed experiment, E-91-016, *Electroproduction of kaons and light hypernuclei* (J. Reinhold and B. Zeidman, spokespersons).

[11] T. Mart and C. Bennhold, Phys. Rev. C **61**, 012201 (2000).

[12] T. Mart, Phys. Rev. C **62**, 038201 (2000).

[13] S. Janssen, J. Ryckebusch, D. Debruyne and T. Van Cauteren, Phys. Rev. C **65**, 015201 (2002).

[14] G. Penner and U. Mosel, Phys. Rev. C **66**, 055211 (2002); 055212 (2002).

[15] K. H. Glander *et al.*, Eur. Phys. J. A **19**, 251 (2004)

[16] R. Bradford, R. A. Schumacher, J. W. C. McNabb and L. Todor [CLAS Collaboration], arXiv:nucl-ex/0509033.

[17] F. X. Lee, T. Mart, C. Bennhold, H. Haberzettl, and L. E. Wright, Nucl. Phys. A **695**, 237 (2001).

[18] M. Q. Tran *et al.*, Phys. Lett. B **445**, 20 (1998).

[19] T. Mart, Ph.D Thesis, Universität Mainz, 1996 (unpublished).

[20] P. M. M. Maessen, Th. A. Rijken, and J. J. de Swart, Phys. Rev. C **40**, 2226 (1989).

[21] Th. A. Rijken, V. G. J. Stoks, and Y. Yamamoto, Phys. Rev. C **59**, 21 (1999).

[22] K. Miyagawa, H. Kamada, W. Glöckle, and V. Stoks, Phys. Rev. C **51**, 2905 (1995); W. Glöckle, K. Miyagawa, H. Kamada, J. Golak, and H. Witala, Nucl. Phys. **A639**, 297c (1998).

[23] K. Miyagawa, H. Kamada, W. Glöckle, H. Yamamura, T. Mart, C. Bennhold, Few-Body

Systems Suppl. **12**, 324 (2000).

[24] A. Nogga, H. Kamada, W. Glöckle, Phys. Rev. Lett. **88**, 172501 (2002).

[25] V. G. J. Stoks, R. A. M. Klomp, C. P. F. Terheggen, and J. J. de Swart, Phys. Rev. C **49**, 2950 (1994).

[26] K. Miyagawa and H. Yamamura, Phys. Rev. C **60**, 024003 (1999); nucl-th/9904002.

[27] X. Li and L. E. Wright, J. Phys. G: Nucl. Part. Phys. **17**, 1127 (1991).

[28] A. Salam, K. Miyagawa, H. Arenhoevel, T. Mart, C. Bennhold, and W. Glöckle, nucl-th/0411036.